Journal Pre-proof

Hierarchical composite coating for enhancing the tensile behaviour of textile-reinforced mortar (TRM)

Cesare Signorini, Antonella Sola, Andrea Nobili

PII: S0958-9465(23)00156-7
DOI: https://doi.org/10.1016/j.cemconcomp.2023.105082
Reference: CECO 105082

To appear in: *Cement and Concrete Composites*

Received date : 30 December 2022
Revised date : 3 March 2023
Accepted date : 16 April 2023

Please cite this article as: C. Signorini, A. Sola and A. Nobili, Hierarchical composite coating for enhancing the tensile behaviour of textile-reinforced mortar (TRM), *Cement and Concrete Composites* (2023), doi: https://doi.org/10.1016/j.cemconcomp.2023.105082.

Hierarchical composite coating for enhancing the tensile behaviour of textile-reinforced mortar (TRM)

Cesare Signorini[a,b,*], Antonella Sola[c], Andrea Nobili[d]

[a]*Institute of Construction Materials, Technische Universität Dresden, Georg-Schumann-Straße 7, 01187 Dresden, Germany*
[b]*Interdepartmental Research Centre CRICT, University of Modena and Reggio Emilia, via Vivarelli 10, 41125 Modena, Italy*
[c]*Manufacturing Business Unit, Commonwealth Scientific and Industrial Research Organisation (CSIRO), Research Way, Clayton, VIC 3168, Australia*
[d]*Department of Engineering "Enzo Ferrari", University of Modena and Reggio Emilia, via Vivarelli 10, 41125 Modena, Italy*

Abstract

We describe a novel class of interface-functionalised textile-reinforced mortar (TRM) composite materials reinforced with basalt and alkali-resistant glass multifilament textiles embedded in a commercially available hybrid lime-cement mortar, usually applied for masonry retrofitting. Spotlight is set on improving the mechanical (tensile) performance of the system through a scalable and easy-to-apply surface treatment for the dry textiles. The treatment consists in soaking the textiles in highly-diluted epoxy resin, to which rice husk ash (RHA) is later added, acting as pozzolanic filler. The resulting functionalised textiles exhibit remarkable adhesion with the matrix owing to the presence of RHA having high specific surface area and rich amorphous content. Three different RHA powders are assessed and their performance is compared to that of plain silica fume. The role of RHA milling is also discussed. The RHA/epoxy coating significantly improves the ulti-

*Corresponding author
Email address: cesare.signorini@tu-dresden.de (Cesare Signorini)

mate tensile strength and energy dissipation capability of the TRMs. In particular, for basalt-textile reinforced composites, the mean tensile strength is three times as much as the uncoated specimens, whereas the dissipated energy at failure is nearly four times as much. Furthermore, the surface treatment qualitatively changes the cracking pattern of the TRMs, for many diffused small cracks appear during tensile testing, and this provides evidence of effective stress distribution in the matrix as a result of superior interphase adhesion.

Keywords: Textile reinforced mortar; Rice husk ash; Epoxy resin; Interface; Tensile test; Basalt fibres; Glass fibres

1. INTRODUCTION

Textile reinforced mortar (TRM) systems belong to a broad class of composite materials often used as externally-bonded reinforcement (EBR) of structural elements. The performance of TRMs is largely affected by the delicate interaction between the reinforcing phase, in the form of woven textiles made of natural (basalt, flax) or synthetic (carbon, glass, polybenzoxazole (PBO), etc.) fibres, and the fine-grained inorganic matrix (usually cement or hydraulic lime mortar).

In spite of the increasing success of TRMs, mortar contains a high volume fraction of solid phases, such as sand, and this is often responsible for the inefficient impregnation of the multifilament yarns. In fact, the average particle size of sand and other solid phases is generally finer in TRMs than in other applications. Nonetheless, it is still significantly coarser than the average distance between adjacent fibres in the bundles, which is in the order of a few microns. Many studies have extensively documented this issue, which is known to limit the real load bearing capacity of the reinforcement [1, 2, 3]. Indeed, this unsatisfactory im-

pregnation usually results in a typical failure mode, which may be described as "telescopic". While the fibres in the sleeve of the bundle are physically or chemically bonded to the cementitious matrix, the fibres at the core of the bundle are free to slide under tensile load [4]. This pseudo-frictional failure mode is also associated with a toughening effect, as the collapse of the textile does not occur abruptly. Even if the sleeve fibres of the bundle eventually break under tensile stress, the core fibres keep sliding and this pseudo-frictional process extends the load transfer over a relatively wide range of displacement [5]. Nonetheless, under telescopic failure, the core fibres cannot be loaded to their maximum strength, and hence they cannot express in full their reinforcing effect. Ultimately, this largely outweighs the benefit coming from pseudo-frictional toughening. Moreover, crack diffusion along the longitudinal axis of the composite system is very limited, and this favours the formation and growth of a few large cracks in the matrix. As a consequence, aggressive agents may penetrate through such cracks, and contribute to deteriorating the composite overlay and its interface with the substrate [6, 7, 8].

Over the last two decades, several strategies have been proposed to increase the efficiency of TRMs. The most straightforward pathway consists in matrix modification, often through the addition of polymers up to the 5% threshold that is prescribed by relevant guidelines [9] (in such case the composite is often named fabric-reinforced cementitious matrix, or FRCM). Yet, the advantage associated with the dispersion of the polymeric admixture in the inorganic matrix remains limited, owing to the fact that only the polymer fraction in close proximity with the textile yarns is really effective. In this sense, a high polymer content would be required for inducing any significant improvement in the TRM response. More-

over, the presence of admixtures may lead to higher water contents than normal, and requires the adoption of defoamers [10].

As a more direct approach at improving the mechanical response of TRM systems, both organic and inorganic coatings may be applied to the textile surface for fostering the chemical and mechanical interaction with the surrounding medium. In general, polymer-based coatings are able to penetrate the textile yarns, reach the core filaments and hold them together for optimal stress distribution [11]. Likewise, organic coatings are very effective at preventing telescopic failure [12]. Moreover, drawing on the solid background developed for fibre-reinforced polymer (FRP) systems [13, 11, 12], polymer sizings are useful for healing defects on the fibre surface, hence improving tensile performance and durability of the composite [14]. It has been argued that polymers are generally sensitive to heat. However, the thermal resistance of the coating actually depends on its formulation [13, 12]. Meanwhile, it has been demonstrated that the inorganic matrix successfully shields the polymeric coating from the deterioration associated with high temperature exposure from the environment [15]. In spite of these advantages, dealing with polymers and resins, e.g., epoxies, may pose technical challenges, especially in light of their high viscosity. In this regard, Signorini et al. [16] developed a new dilution protocol that warrants better impregnation of the textile, owing to viscosity optimisation.

Conversely, inorganic coatings, which are typically based on the deposition of micro- or nano-silica particles, offer the considerable advantage of matching the purely inorganic nature of TRMs [17, 3, 18, 19]. The rationale behind the choice of applying an inorganic coating is the delivery of particles with a highly amorphous structure, mainly silica, at the interface between the fibres and the

hydraulic matrix, where they are capable of triggering pozzolanic reactivity [20, 21]. However, the synthesis of silica generally involves significant costs and leads to a moderate, but not negligible, environmental footprint, mainly because of the extensive use of organic solvents [22].

Biomass ashes, especially rice husk ash (RHA), can be coated at the textile-mortar interface as an environmentally-friendly alternative to synthetic silica. At present, owing to its rich amorphous fraction, RHA is being researched in blended binders, in order to partially replace ordinary Portland cement (OPC) [23, 24, 25]. However, despite the large abundance of RHA, especially in Asia, the availability of this agricultural by-product is largely insufficient to meet the huge demand by the concrete industry. The idea of delivering RHA at the textile-mortar interface makes it possible to harness its reactivity while reducing the required volumes. To the Authors' knowledge, this is still a new area of research, with very few examples being available in the literature.

The preliminary study by Sola et al. [26] assessed the effectiveness of two polyvinyl alcohol (PVA)-based coatings, loaded with either RHA or with a 50/50 mixture of RHA and silica fume (SF). These coatings were applied to basalt textiles embedded in TRM coupons, which were tested under uniaxial tensile loading. Although both coatings were able to increase the loading capacity of the composite, the improvement was approximately 20% with RHA, and just 7% with the RHA/SF mixture.

Moving from these promising results, this paper compares the reinforcing capability of three types of RHA powders, which differ by the rice husk variety they are obtained from and by the combustion process they go through. Although the investigated RHA powders are being presently diverted to the iron and steel in-

dustry, their production rate far exceeds the demand, and this calls for new valorisation strategies. To this end, a thorough investigation is carried out to assess the potential of RHA powders to work as reactive materials at the interface between mortar and textile in TRM composites. Based on this preliminary investigation, the most promising RHA is then milled, sieved and then applied to either basalt or glass textiles, using a highly diluted epoxy resin as carrier. Uniaxial tensile tests conducted on 1-ply TRM coupons clearly demonstrate that the mechanical behaviour of the coated textiles is far superior to that of the control group, in terms of both strength and energy dissipation. This improvement is reflected by the failure mechanism, which transitions from single to diffuse cracking for the functionalised specimens.

2. MATERIALS AND METHODS

2.1. Raw materials

The matrix is a commercial pre-mixed lime-based mortar (Kerakoll S.p.A., Geocalce Fino®) intended for structural retrofitting of masonry elements. The physical and mechanical properties, as declared by the manufacturer, are listed in Table 1 [27]. This matrix was previously studied by Signorini et al. [16] and to this work we point for further details.

The structural reinforcement was either an open-square grid basalt textile (labelled “B" hereafter), received without any sizing, or an open-square grid alkali-resistant glass textile (“G"), where a zirconium oxide (ZrO_2)-based sizing provides the fibres with chemical stability in alkaline environment. Table 2 gathers some technical specifications for the textile reinforcements, as declared by the manufacturers.

Table 1: Properties of the lime-based repair mortar, as provided by the manufacturer [27].

Property	**Unit**	**Value**
Binder	—	Natural hydraulic lime (NHL 3.5)
Aggregates	—	Silicate and carbonate
Particle size range	mm	$\leq$1.4
Final density	$\mathrm{g\,cm^{-3}}$	1.58
Char. compressive strength (28d)	MPa	15
Char. bending strength (28d)	MPa	5
Char. bond strength (28d)	MPa	1

Table 2: Specifications of the basalt (B) and glass (G) textiles.

Property	**Unit**	**B**	**G**
Grid spacing	mm	17	12
Mass per unit area	$\mathrm{g\,m^{-2}}$	200	300
Specific weight (fibres)	$\mathrm{g\,cm^{-3}}$	2.60	2.50
Elastic modulus	GPa	62	74
Ultimate tensile strength (dry)	MPa	3000	1400
Equivalent thickness	µm	32	60

Three different RHA powders were provided by Curtiriso S.r.l. for this pilot study on the upcycling of materials coming as by-products of the rice industry. The CL and GA powders ("CL-RHA" and "GA-RHA", respectively) are produced from the combustion of rice husk in fix-grid furnaces. The rice quality for CL-RHA is parboiled, whilst GA-RHA comes from a mixture of parboiled rice (prevailing fraction) and white rice (minor fraction). The CU powder ("CU-RHA") is obtained in a furnace working at higher temperature. Both combustion plants have the primary function of providing heat for parboiling the paddy in the company's rice mills. Being sensitive information, no further detail can be disclosed regarding the production process of the different RHAs. In order to evaluate the effect of the particle size, GA-RHA is dry-milled in a planetary mill

for $10\,\mathrm{min}$ using a porcelain jar loaded with alumina balls, and then sieved below $100\,\mu\mathrm{m}$ ("GA-RHA-G").

For the sake of comparison, a commercially available undensified SF powder (Microsil DM, AZ Tech Srl, Italy, "SF") is investigated as benchmark. This fume is obtained in electric arc furnaces from the reduction process of quartzite for the production of ferro-silicon or silicon metal alloys. It consists of SiO_2 in excess of 85% and its density ranges between 450 and $650\,\mathrm{kg\,m^{-3}}$. This kind of SF is currently used in practice as a filler in lightweight cement-based conglomerates.

2.2. Preparation of the tensile test specimens

2.2.1. Surface modification of the textiles

Both B and G textiles were cut-to-size for manufacturing individual tensile coupons. Textile specimens measured $450\,\mathrm{mm}$ in length and $50\,\mathrm{mm}$ in width, the latter being an integer multiple of the grid spacing (specifically accommodating 3 yarns for B textiles and 4 yarns for G textiles). The pre-cut textile strips were pre-treated in a 2 wt.% aqueous solution of (3-aminopropyl) triethoxysilane, APTES (99%, Sigma-Aldrich) because, as discussed by Messori et al. [12], this improves the chemical interaction between the (inorganic) fibres and the (organic) coating. After drying at room temperature, the textile strips were coated with dilute epoxy resin. The epoxy coating (acting as "glue" for the RHA particles as explained below) was obtained by diluting high-purity bisphenol A diglycidylether (D.E.R. 332, DOW Chemicals) with technical acetone ($(CH_3)_2CO$, Incofar S.r.l.) at 75% wt:wt and then curing with the aliphatic hardener diethylenetriamine (DETA 99%, Alfa-Aesar) in stoichiometric ratio. The details of the dilution and coating procedure can be found in Signorini et al. [16]. It should be noted that, in this study, an aliphatic hardener was preferred to an aromatic hardener in order to provide the

epoxy resin with higher ductility [12].

Each textile strip was thoroughly bathed in the solution, then squeezed out to remove excess coating and finally pressed onto a powder bed of the selected RHA filler. For each strip, this operation was carried out on each side, and ultimately the excess filler was gently shaken off. The textile strips were laid down flat on a polypropylene (PP) film and let to cure under ambient conditions for 7 days. Figure 1 shows both the B and G textile strips before and after curing.

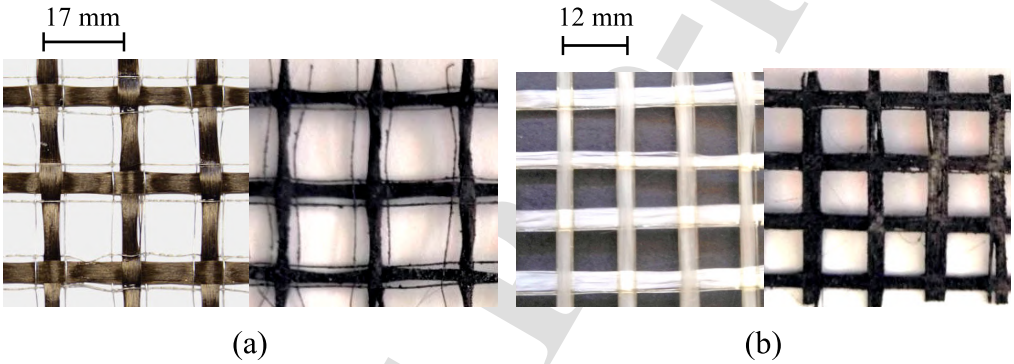

Figure 1: B (a) and G (b) textile strips are compared in the as-received state (left) and after complete reticulation of the coating (right).

2.2.2. Specimen manufacturing for tensile testing

Rectangular coupons for tensile testing were produced one-by-one in a polyethylene (PE) formwork specifically designed for the purpose, to avoid cutting from a larger sheet. This formwork ensures that the specimen's thickness is uniform and that the pre-cut textile is consistently placed at the mid-plane, as discussed by Messori et al. [12]. As illustrated in Figure 2, the workflow encompasses the following operations:

1. 3 mm-thick PE spacers are nailed to the PE board at constant spacing corresponding to the width of the coupons (Figure 2a);

2. a first layer of mortar is poured onto the formwork and levelled up with a scraper to the spacer's thickness (Figure 2b);

3. the cut-to-size textile is placed onto the mortar and gently pressed to ensure mortar penetration in the grid spacings (Figure 2c);

4. a second set of PE spacers is fixed on top of the first one to reach the final specimen thickness (Figure 2d)

5. a second layer of mortar is poured into the formwork and levelled up (Figure 2e)

6. the top surface of the specimens, neatly arranged in the formwork, is eventually levelled with a trowel to remove the excess of mortar (Figure 2f).

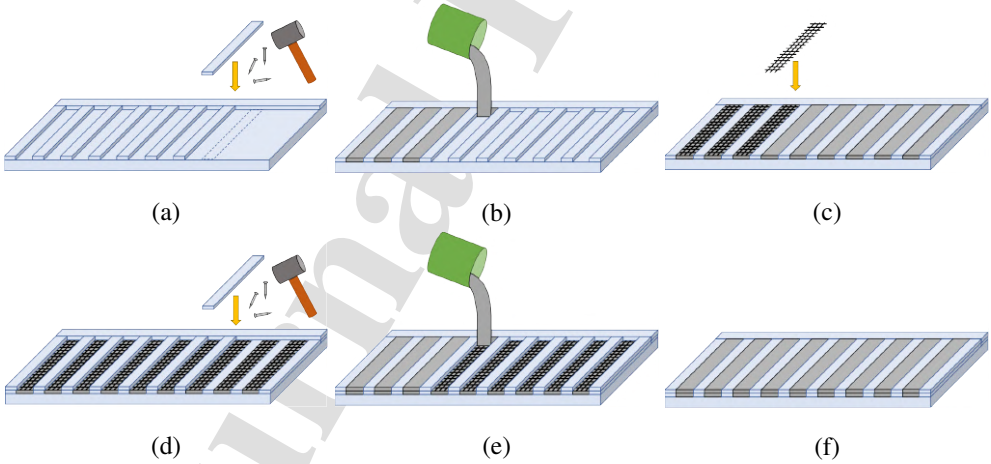

Figure 2: Procedure for fabricating individual 1-ply TRM coupons for tensile testing.

According to the ICC acceptance criteria [28], in order to minimise specimen warping due to differential water evaporation from the top and bottom surfaces, 7-day moist curing is completed in an air-tight PP bag before stripping off the

coupons from the formwork. Moreover, since the curing time is generally recognised as a key driving parameter of mechanical performance [29], extended 56-day curing in ambient conditions is accomplished for all specimens. This offers a more realistic representation of the final material performance than the traditional 28-day curing time. Finally, 100 mm-long glass textile tabs are epoxy glued to the ends of each specimen to accommodate the clamps of the testing machine.

To better appreciate the role of the coating, the same procedure is precisely replicated to manufacture coupons reinforced with *uncoated* B and G textiles. In the following, for the sake of brevity, we shall distinguish between “coated" and “uncoated" specimens, with the understanding that the former employ RHA/epoxy.

The specimen gauge length L_g equals $250\,\mathrm{mm}$ for all specimens. As customary, stress is computed dividing the load by the textile reinforcement area (A_f), specifically $3.0\,\mathrm{mm}^2$ for G, and $1.6\,\mathrm{mm}^2$ for B.

2.3. Testing protocol

2.3.1. Powder characterisation

For each RHA variety investigated in this study, about 8-10 g of powder were collected directly from the same powder bed which was subsequently used for coating the fabrics. Particles were taken from different points of the powder bed and across its thickness, in order to obtain a representative sample. Each powder sample was then stored in a sealed flask and mixed thoroughly prior to each measurement.

The morphology of the as-received RHA and SF powders was assessed in a scanning electron microscope (SEM, FEI Quanta, The Netherlands). Field emission gun scanning electron microscopy (FEG-SEM, Nova NanoSEM 450, FEI Quanta, The Netherlands) was also used for investigating finer microstructural

features. The particle size distribution was determined with a laser granulometer (Mastersizer 2000 Ver. 5.22, Malvern Instruments Ltd., Malvern, UK).

After calibration, each powder sample was added to the dispenser as prompted by the instrument in order to reach an ideal signal based on the "obscuration" (i.e., the fraction of light lost) from the analyser beam [30]. Each curve showing the granulometric size distribution is thus representative of the particle size distribution of the corresponding powder as a whole, as determined under the best acquisition conditions. SEM inspection and particle size determination were repeated on GA-RHA after milling.

X-ray diffraction spectra (XRD, X'pert PRO, PANalytical, Almelo, The Netherlands) were acquired in the 5-120° 2θ range, with a step size of 0.0167° 2θ and a scan step time of 22.225 s, using the CuKα radiation (λ = 1.54 Å). Fourier transform infrared spectroscopy (FT-IR Vertex 70, Bruker, Germany) in attenuated total reflectance (ATR) mode was employed to compare the chemical functionality of the powders.

Finally, the specific surface area (SSA) was measured by N_2 adsorption and desorption at 77 K on a Micromeritics Gemini V2.00 instrument. The N_2 isotherms were used to calculate the SSA by applying the Brunauer-Emmett-Teller (BET) method. Along with the SSA, the instrument automatically estimates the error of the BET surface area. Powder samples for measuring the SSA weighted approx. $0.9\,\mathrm{g}$. The same technique was also applied to measuring the SSA of the textiles. Due to the destructive nature of the test, the SSA of the textiles, before and after coating, was determined on one sample only (with mass of about 0.9 g) for each reinforcement. Samples were chosen to be representative of the corresponding textiles.

Table 3: Testing protocol for tensile characterisation of TRM composite coupons

Textile	**Pre-treatment**	**Label**	L_g [mm]	A_f [mm^2]	**Repetitions**
AR-glass	None	G-NC	250	3.0	5
	Epoxy + GA-RHA-G	G-RHA			5
Basalt	None	B-NC	250	1.6	5
	Epoxy + GA-RHA-G	B-RHA			5

2.3.2. Mechanical testing of TRM composites

1-ply specimens were tested on the universal testing machine (UTM) Instron 5567, equipped with a $30\,\mathrm{kN}$ load cell. Specimen clamping was realised through wedge grips. This set-up corresponds to type A, as described by Hartig et al. [31], under the heading “rigid load application". Although clevis grips are sometimes preferred for investigating the bond strength in TRMs, wedge grip clamping is also in use. Indeed, following Nerilli and Ferracuti [32], wedge grips provide a more uniform stress distribution over the specimen cross-section and, therefore, allow for a robust evaluation of the constitutive tensile law of the TRM. This clamping system also complies with the RILEM 232-TDT protocol [33], which recommends to apply sufficient lateral pressure to prevent textile slippage, as opposed to clevis-type grips which only apply longitudinal force [34]. To capture the softening behaviour, tensile tests were carried out under displacement control at the nominal displacement rate of 0.50 $\mathrm{mm/\,min}$.

3D Digital Image Correlation (DIC) was adopted during testing to record the displacement field on the speckled specimen surface (Q-400, Dantec Dynamics, Germany). The software GOM Correlate (GOM Italia S.r.l., Zeiss Company, Italy) was used to investigate the crack patterns and to assess the actual speci-

men elongation by subtracting the clamping system's elongation. Finally, failed specimens were qualitatively investigated in order to ascertain the role of interface modification on the failure mode. The testing protocol is summarised in Table 3.

3. RESULTS AND DISCUSSION

3.1. RHA powders

The three RHA powders here investigated were first screened to identify the most promising candidate to be introduced at the mortar-to-textile interface. Results were compared to those obtained with undensified SF, which is taken as benchmark on account of its well-known pozzolanic activity [17, 18].

The physical properties of the RHA powders are mainly determined by the rice source and by the combustion process. At low magnification (first column in Figure 3), they all look alike and appear as lamellar fragments, either flat or slightly curled up, with one side smooth, and the other side typically rough and wavy. Moving to greater magnification (middle column in Figure 3), it can be appreciated that, whilst the raised pattern of the wavy side of CL-RHA and CU-RHA is mainly bumpy, the GA-RHA powder is actually different, as the textured side presents an extremely complex comb-like architecture, with elongated crests and deep pores. Working at even greater magnification (last column in Figure 3), relevant differences also emerge between CL-RHA and CU-RHA, since the surface of the bumps in CU-RHA is sensibly more porous than that of CL-RHA. Moreover, for CL-RHA, the grooves between adjacent waves appear more shallow and continuous than those visible in CL-RHA.

Although the lamellae may be as large as $500\,\mu\mathrm{m}$, the structured surface and the micro-porosity may be advantageous in providing the as-received RHA powders with a large SSA, as confirmed by the data in Figure 4. Assuming d_{50} as the

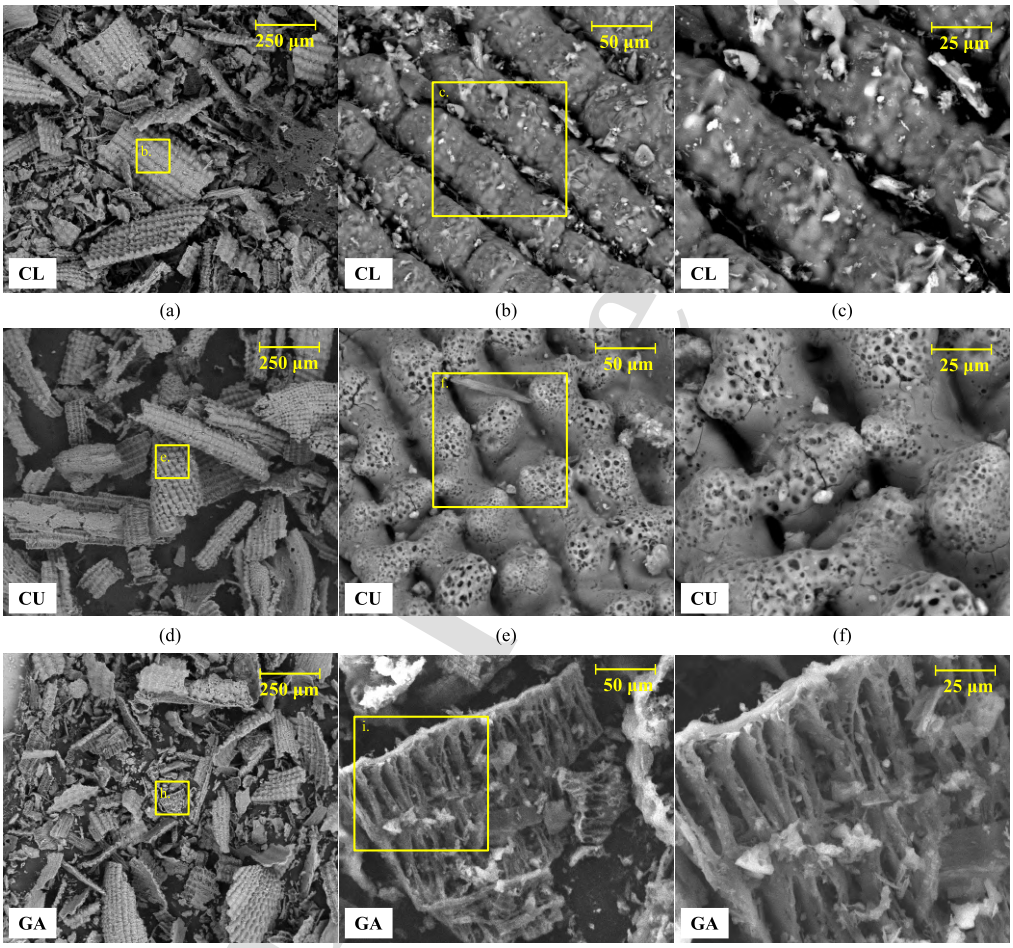

Figure 3: SEM images of the RHA powders (as-received) at different magnification levels.

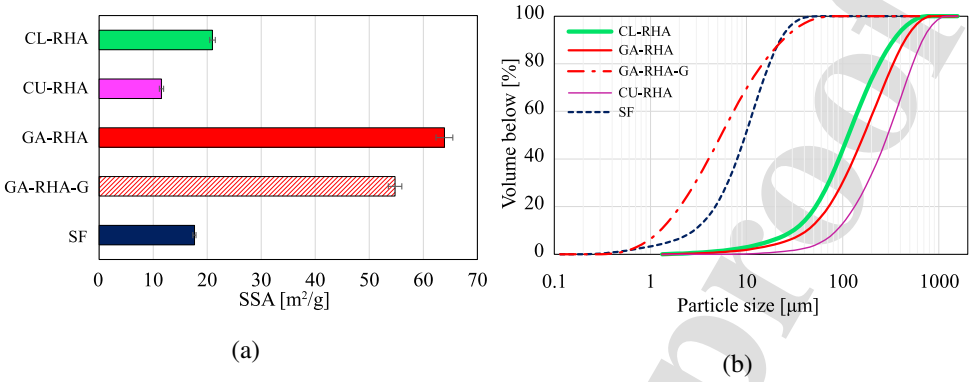

Figure 4: Specific surface area (SSA) and particle size distribution of the active fillers.

representative index for the average particle size, it is clear that the average size of CL-RHA (d_{50} = 146 µm), which is the finest among the considered RHA powders, remains one order of magnitude bigger than that of SF (d_{50} =12 µm). Nonetheless, the SSA of CL- and CU-RHA powders is comparable to that of SF. Interestingly, the SSA of GA-RHA is exceptionally high, and largely exceeds that of SF by a factor of four. This remarkable outcome likely originates from the unique comb-like surface of GA-RHA lamellae, wherein the extremely thin filaments and deep recesses create a texture remindful of the pecten observed in seashells and other natural constructs [35].

FT-IR spectra are reported in Figure 5. Following Kumpfer Nascimento [36], the strong absorption located at around 1045 cm^{-1} can be attributed to asymmetric stretching of Si-O-Si bonds, while the peak at 795 cm^{-1} may be due to their symmetrical stretching. Interestingly, the weak absorption observed at 618 cm^{-1} is characteristic of crystalline cristobalite. Similar peaks can also be identified in the SF spectrum, where, however, the absorption peak of cristobalite is absent.

Figure 6 compares the peaks in the diffraction spectra of the RHA powders

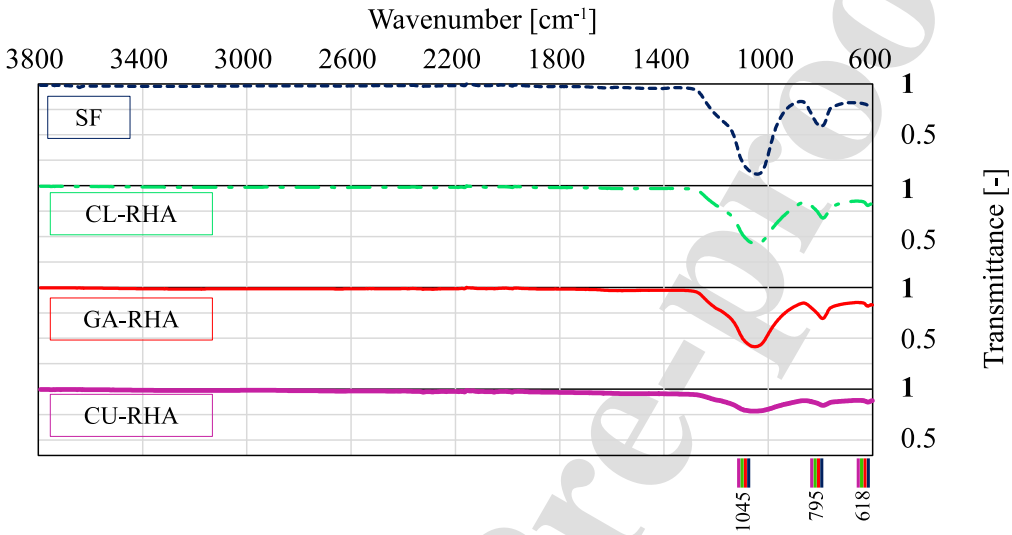

Figure 5: FTIR spectra of RHA powders in comparison with SF.

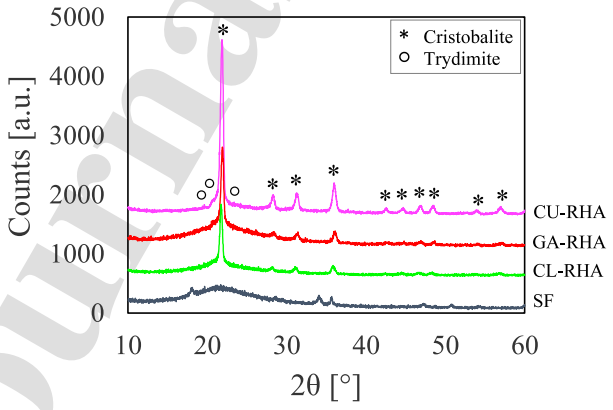

Figure 6: XRD spectra of RHA powders in comparison with SF.

against cristobalite (JCPDS PDF No. 39-1425) and tridymite (JCPDS PDF No. 42-1401). It is known from the literature that long-time exposure to high temperature in the combustion process may lead to the formation of crystalline polymorphs of silica [37, 38]. Nonetheless, the RHA powders still exhibit a rich amorphous phase, as demonstrated by the broad band in the angular range between 10° and 35° 2θ, which is typical of amorphous silica [39]. The comparison of the RHA spectra in Figure 6 suggests that the amorphous phase should be particularly abundant in GA-RHA. Conversely, CU-RHA is the most crystallised powder, most likely because it is produced at high temperature in a different incineration furnace. Significantly, as pointed out in the literature Rivas et al. [37], Shinohara and Kohyama [38], besides the burning conditions, the presence of potential impurities in the rice husk, such as K_2O or P_2O_5, may also affect the crystallisation. In contrast, SF is entirely amorphous, with minor peaks likely due to the presence of contaminants. Although the identification of these minor phases is questionable, due to the weak intensity of the corresponding peaks, we may still tentatively link them to silicon carbide (as previously detected, for example, by Arroudj et al. [40]) and to portlandite, which is a hydrated form of calcium oxide (as per the diffractogram reported, for example, by Cárdenas-Escudero et al. [41]), with silicon carbide and calcium oxide being recognised as common contaminants in silica fume [42].

Based on this preliminary characterisation, GA-RHA stands out as the best option for textile functionalisation on account of the fact that it presents the highest SSA and richest amorphous fraction among the investigated RHAs. However, concerns may still arise from its relatively large particle size, which may affect the thin nature of the coating in close adhesion to the textile yarns. Precisely to

mitigate this issue, GA-RHA powder was dry-milled for $10\,\mathrm{min}$ and sieved below $100\,\mu\mathrm{m}$. The particle size analysis repeated on the milled powder (GA-RHA-G in Figure 4(a)) demonstrates that RHA can be easily comminuted due to its brittle behaviour, as already reported by Chindaprasirt et al. [43]. Consequently, milling for $10\,\mathrm{min}$ was sufficient for cutting down the average particle size of GA-RHA from around 212 $\mu\mathrm{m}$ to around 7 $\mu\mathrm{m}$, leaving marginal quantities of coarse powder trapped by the sieve. Thus, after milling, the average particle size of GA-RHA-G was nearly half of that of SF (around 12 $\mu\mathrm{m}$, as seen before), although the particle size distribution remained broader. Somewhat surprisingly, the SSA of GA-RHA-G was slightly reduced after milling (Figure 4(b)), in spite of the GA-RHA particles becoming much finer. One possible explanation is that the milling process likely damages the delicate pecten structure of the as-received GA-RHA powder. As a result, the increase in SSA due to comminution is outweighed by the damage to the fine microstructural features. Indeed, similar outcomes after milling have already been observed by other authors, for example by Mehta [44]. Also, this explanation is supported by the FEG-SEM analysis in Figure 7, where the fragmentation of the original GA-RHA lamellae in sub-micron particles and the damage to the comb-like structure can be clearly appreciated. As compared to SF, GA-RHA-G particles are jagged and sharp-edged, due to brittle breakage of the GA-RHA lamellae. Both GA-RHA-G and SF are prone to agglomeration, as a result of their sub-micron size [45]. Notwithstanding the unexpected decrease of SSA due to milling, the specific surface of GA-RHA-G is still three times as much as SF (Figure 4(b)). Meanwhile, the substantial reduction in the average particle size is certainly beneficial for a successful coating deposition. In light of these reasons, GA-RHA-G is finally selected as the best candidate for the mechanical

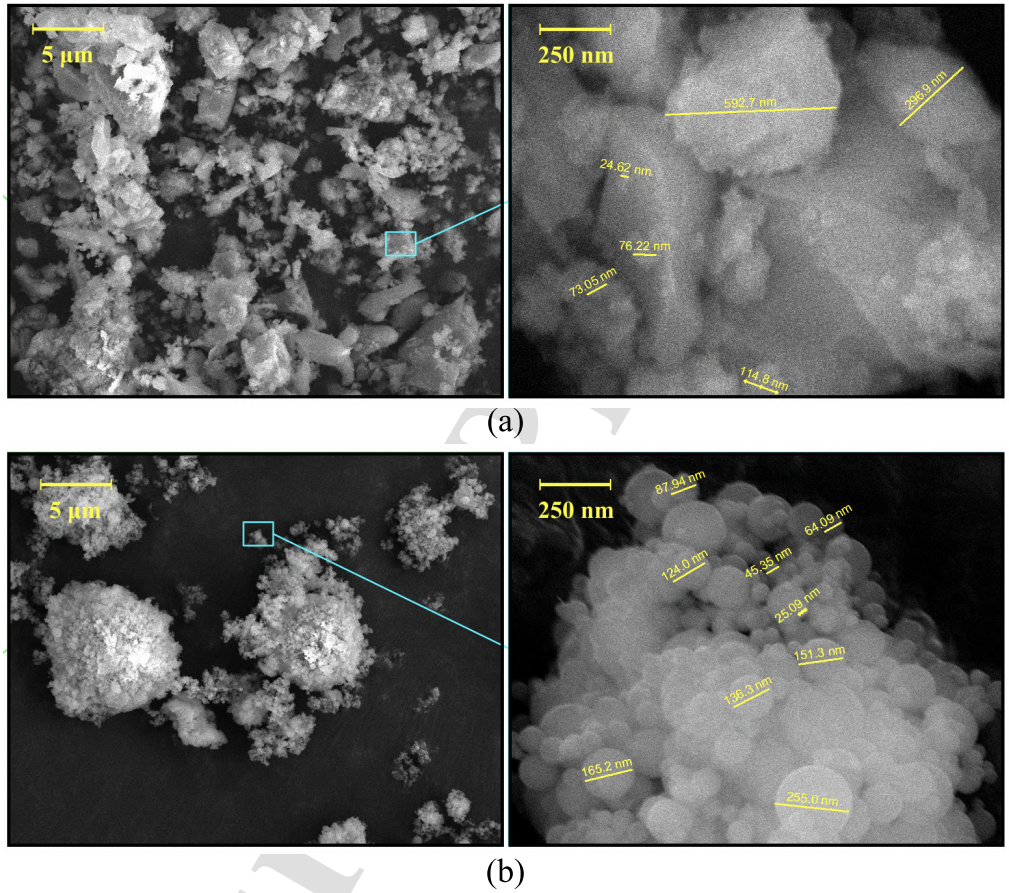

Figure 7: FEG-SEM images of GA-RHA-G (a) and undensified SF (b).

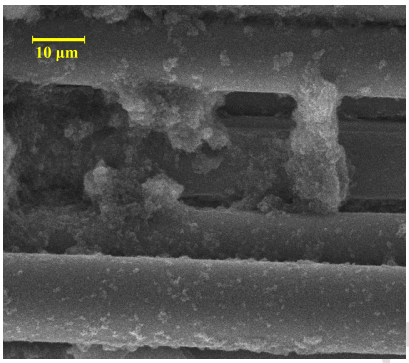

Figure 8: SEM image of a GA-RHA-G/epoxy coated G-textile before embedding in mortar. Similar microstructure was observed for GA-RHA-G/epoxy coated B-textile

assessment of the TRM coupons.

3.2. Microstructure of interface-modified TRM composites

Whereas RHA is commonly used in building materials as a partial replacement for OPC [46], in the present contribution it is investigated as a functional filler whose role is to promote the otherwise weak interaction between the mortar and the reinforcing textile in TRM composites. In this context, RHA consumption is marginal, for it only acts as a component of the epoxy-based coating of the textile. As shown by Figure 8, SEM inspection reveals that GA-RHA-G particles are evenly distributed on and tightly adhering to the fibres' surface, with the epoxy resin working simultaneously as gluing agent and protective coating.

As illustrated by the schematic diagram of Figure 9, interface modification results in a hierarchical composite, since the textile provides structural reinforcement at the macro-scale, given that the typical length-scale of the mortar-textile composite system is in the order of centimetres, while the hybrid coating plays a role at the micro-scale, in the scale of microns. The composite coating has been designed in order to take full advantage of the manifold functional features of both

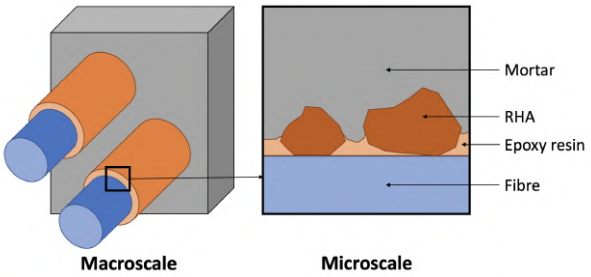

Figure 9: Multiscale hierarchical structure of the interface-modified TRM composites.

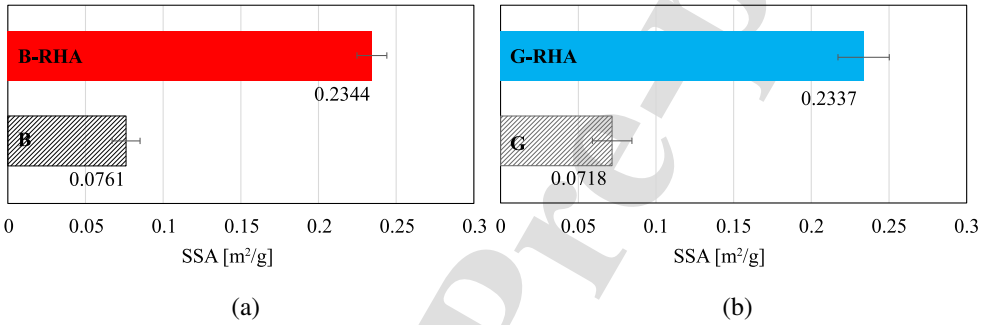

Figure 10: Specific surface area (SSA) measured for B- and G-textiles before (labelled “B" and “G") and after (labelled “B-RHA" and “G-RHA") receiving the GA-RHA-G/epoxy coating.

the epoxy matrix and the RHA particles. The epoxy resin fulfils two main purposes: on the one hand, it glues the RHA particles onto the surface of the fibres; on the other hand, it hinders telescopic failure by bridging yarns together (see also the contribution by Messori et al. [12]). Owing to the special coating process, whereby epoxy is applied first and then the textile is dipped in the functional powder, RHA particles, while glued to the surface of the textile, are directly exposed to the surrounding matrix. As such, they enhance friction and offer a wide active surface for the pozzolanic reactions to occur (which, according to the results published by Jamil et al. [47], are favoured by fine particles with high SSA).

The substantial increase in SSA associated with the presence of the composite

coating is confirmed by the data in Figure 10. Regardless of the nature of the fibres, be they either B or G, the SSA of textiles functionalised with the GA-RHA-G/epoxy coating scores around three times as much as that of the uncoated textiles. This observation supports previous results concerning B textiles treated with a RHA/PVA composite coating [26]. The availability of a wide surface area is expected to favour interaction with the surrounding mortar, and thus improve interface adhesion.

3.3. Tensile behaviour

3.3.1. Basalt textile-reinforced TRM (B-TRM)

Figure 11 plots the stress-strain ($\sigma - \varepsilon$) curves obtained for all B-TRM specimens, with and without functional coating. Specimens reinforced with bare (uncoated) B textiles generally fail through sliding right after the first macro-crack appears in the matrix, due to poor bonding at the interface between the textile and the matrix. It is also worth mentioning that a contributing factor to this unsatisfactory behaviour may be given by progressive deterioration of the fibres as a result of direct exposure to the strongly alkaline environment of the surrounding matrix. Poor stability in the alkaline environment is indeed a well-known issue with basalt fibres [8, 48].

The curves of the uncoated specimens illustrate three regimes, namely linear elastic, matrix micro-cracking and, finally, macro-crack formation with textile sliding. Although micro-cracking may sometimes occur with a modest increase in strength, the global behaviour is that of fragile matrix failure followed by friction-dominated textile delamination, both phenomena being rather inconsistent, as it appears in the different shape that curves take in Figure 11(a). In contrast, epoxy coating, despite being very thin as a result of acetone dilution

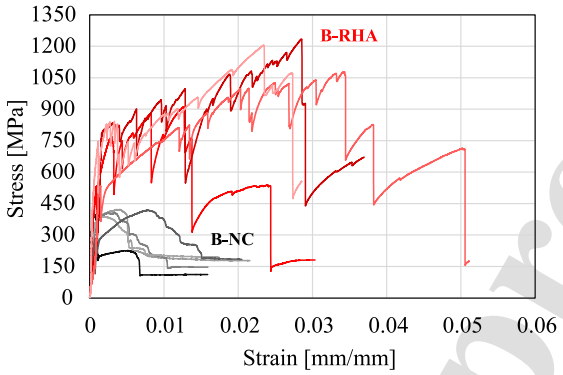

Figure 11: Stress-strain curves of B-TRM composites, with ("B-RHA", red) and without ("B-NC", black) GA-RHA-G/epoxy coating, subject to uni-axial tension.

[16], is able to form a continuous barrier that surrounds the fibres' surface, as in Figure 8. Owing to its relatively good chemical stability [49], the epoxy coating shields and protects the fibres from the alkaline environment. GA-RHA-G particles offer additional sheltering, promote pozzolanic reaction and ultimately increase the mortar-to-textile bonding quality at the interface. This is supported by the enhanced strain-hardening behaviour of the coated B-TRM specimens, which usually fail after multiple micro-cracks are formed. This is ultimately associated with an even damage distribution in the matrix. This loading process is clearly seen through the repeated stress drops appearing in the curves of Figure 11.

As shown in Figure 12, the quality of the adhesion between the coated textile and the hydraulic matrix is further documented by the existance of diffused mortar patches strongly attached to the textile yarns after testing.

The bar-charts of Figure 13 best summarise the striking improvement that textile coating and textile-to-matrix interface modification offer to mechanical performance. Indeed, the bar-charts in Figure 13 compare the mean and the characteristic values of the tensile strength (f_t) and the dissipated energy at failure (W)

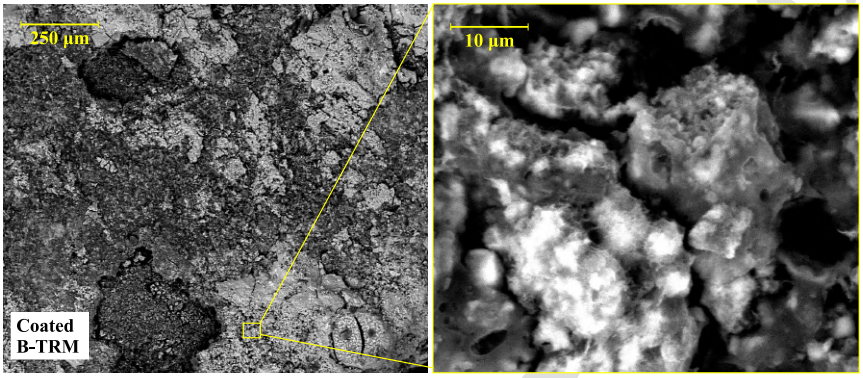

Figure 12: SEM images of the fracture surface of failed B-TRM

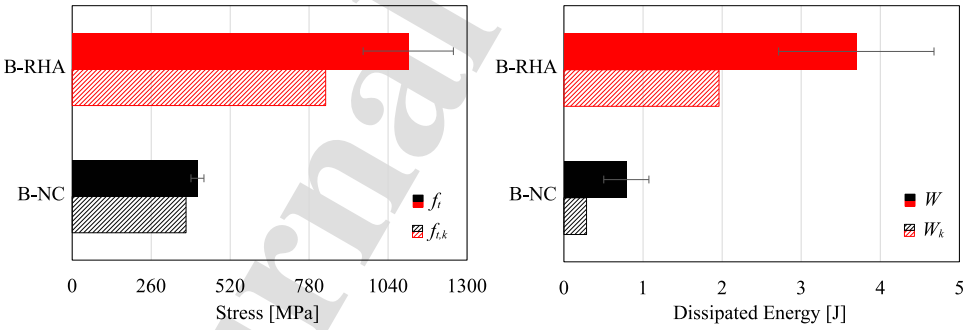

Figure 13: Bar-charts showing the mean values and the characteristic values (subscript "k") of the tensile strength ("f_t") and the dissipated energy at failure ("W") for B-TRM specimens with ("B-RHA") and without ("B-NC") GA-RHA-G/epoxy coating.

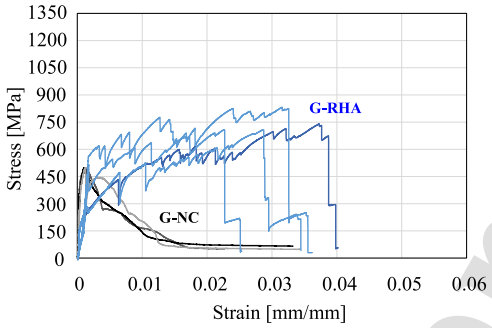

Figure 14: Stress-strain curves of G-TRM composites, with ("G-RHA", blue) and without ("G-NC", black) GA-RHA-G/epoxy coating, subject to uni-axial tension.

for B-TRM composites with and without GA-RHA-G/epoxy coating. ± 1 standard deviation (ζ) bands are also shown to represent data scattering. The dissipated energy at failure is calculated as the area under the load-displacement curves and combines strength and ductility in a single index [8]. The characteristic value, indicated with the subscript "k", is determined, assuming a normal distribution, according to the so-called "2-sigma rule" (that is in conjunction with a 95% confidence interval)

$$(\cdot)_k = \mu(\cdot) - 1.96\zeta(\cdot)$$

In other words, the characteristic value of a random variable normally distributed is exceeded 95% of times [50]. According to the bar charts, both the mean tensile strength and the mean dissipated energy exhibit an almost three-fold increase when the B textiles are coated with the GA-RHA-G/epoxy system. By the covariance phenomenon, data scattering is also increased and this is reflected by the characteristic values. Yet, the overall effect remains remarkably positive for both indices and this outcome makes a strong case in favour of coating application.

3.3.2. Glass textile-reinforced TRM (G-TRM)

Figure 14 compares the stress-strain curves of the individual G-TRM specimens, with and without coating. As already seen for B-TRM, under tensile loading, the mechanical response of the G-TRM specimens with and without coating is completely different, with the coated samples significantly outperforming the uncoated oes. As previously mentioned, in the absence of coating, textile yarns are easily pulled out of the surrounding matrix due weak interface bonding. However, unlike the basalt counterparts, the tensile behaviour of the uncoated G-TRM specimens remains well consistent, so much so that single stress-strain curves are, for the most part, almost identical. This consistency is somewhat unusual, given that TRM composites are delicate systems whose performance is governed by several factors, many of which cannot be perfectly controlled (such as the presence of defects). Flaws, which are randomly distributed over the gauge length, act as crack initiation points and therefore their number and location cause strong variability [51]. In the case of the uncoated G-TRM specimens, instead, the first crack occurs in the mortar at almost the same stress level for nearly all tests. Subsequently, as the applied load increases, softening kicks in given that the bearing capacity is now governed by textile friction and progressive delamination. In contrast, the presence of the coating promotes strain-hardening because, after the first crack occurs, the textile is well engaged and this allows more cracks to develop. However, the strain-hardening is less pronounced than that previously observed for the B textiles, most likely because G fibres are weaker and more compliant than B fibres [52]. It is also worth mentioning that, besides triggering a different failure mode, the presence of the GA-RHA-G/epoxy coating slightly increases the first crack stress (FCS), possibly because the enhanced bonding at the textile-

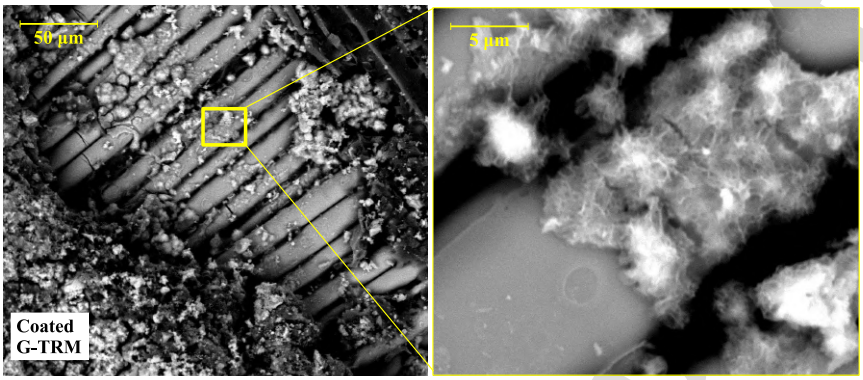

Figure 15: SEM images of the fracture surface of failed G-TRM

to-matrix interface enables a more efficient load transfer. Interestingly, several studies in the literature investigate the effect of various functional coatings on the FCS. The results may be contradictory, depending on the nature of the fibres and the composition of the coating. For example, highly hydrophilic fibres like jute, when treated with a polymer coating, tend to become hydrophobic. This undermines the fibre-matrix interaction, and ultimately reduces the FCS, with a drop that may be in the order of 20% [53].

In analogy to the results previously discussed for the B-TRM samples, Figure 15 clearly shows well formed acicular hydration products that are firmly attached to the fibre surface in the G-TRM samples, which provides evidence of improved bond quality.

The bar-charts in Figure 16 present the mean and characteristic values of the UTS and the dissipated energy for the G-TRM composites, alongside the ± 1 standard deviation bar. Both the mean value and the characteristic value of the tensile strength of the G-TRM specimens are lower than those of the B-TRM ciunterparts. The gain associated with the presence of the coating, though relevant, is also much less striking. In stark contrast, the improvement in terms of dissipated energy is

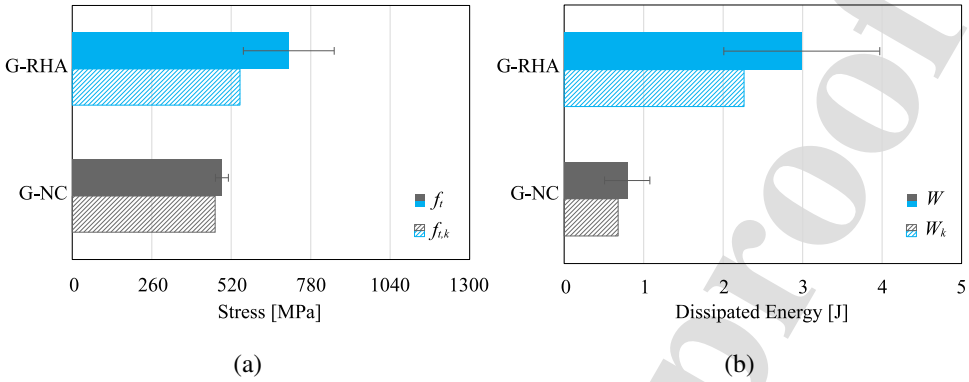

Figure 16: Bar-charts showing the mean and the characteristic value (subscript "k") of the tensile strength ("f_t") and of the dissipated energy at failure ("W") for G-TRM specimens with ("G-RHA") and without ("G-NC") GA-RHA-G/epoxy coating.

comparable to that attained for the B-TRM samples. In fact, the enhanced bond quality at the interface, which is sustained by the combined effect of the epoxy matrix and the protruding active particles (as evidenced by the SEM photographs in Figure 15), supports a diffuse crack pattern that is similar to that showed by the B-TRM coupons. As a result, the functional coating greatly increases ductility, and, in doing so, ultimately leads to an energy dissipation capability that is more than three times as much as the uncoated group.

3.3.3. Failure modes and comparative analysis of performance indices

Figure 17 presents an overview of the main performance indices for the specimen groups under testing. Shaded areas collect the points expressing the tensile strength (on the abscissa) and the dissipation capacity (on the ordinate axis) of individual specimens and visualise standard deviations. The corresponding characteristic values for the mean are also indicated. Interestingly, the performance of all uncoated specimens is similar, regardless of the reinforcing textile. This observation supports the idea that the textile-to-matrix interface bond governs the

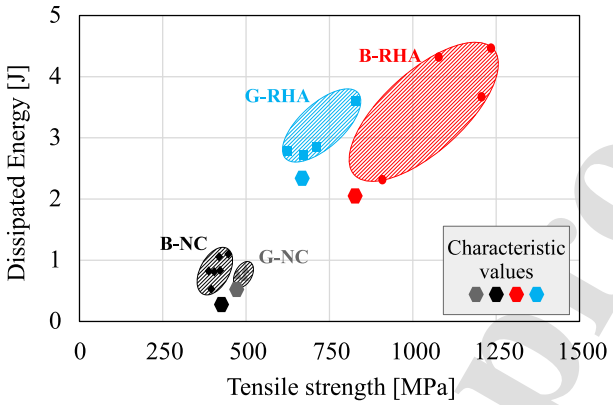

Figure 17: Performance indices for the TRM composites under scrutiny. Small circles indicate individual test results, large hexagons show characteristic values for the mean.

final behaviour of the composite. A weak bond at the interface does not allow to achieve in full the load bearing capacity of more performing textiles. This similarity also extends to the characteristic values and to the failure mode. In fact, due to the weak interaction of the interface, the failure mode is initiated by the formation of a single macro-crack in the mortar, upon reaching its tensile strength in the weakest cross section. Then, the first crack is followed by friction-dominated delamination. In this process, the intrinsic properties of the textile are hardly relevant. An example of this matrix-governed failure can be appreciated in Figure 18, that shows the strain field on the surface of an uncoated B-TRM specimen ("B-UC-1"), as obtained by DIC, at four subsequent stages of the tensile testing. A first crack initiates in the weakest cross section along the gauge length and then widens steadily as the applied load increases, until the specimen eventually fails, with no secondary cracks appearing in the process.

Conversely, the improved interface bond quality typical of coated specimens promotes a more efficient load transfer, that induces a diffuse crack pattern. This is clearly seen, for example, in Figure 19 relating to the coated B-TRM specimen

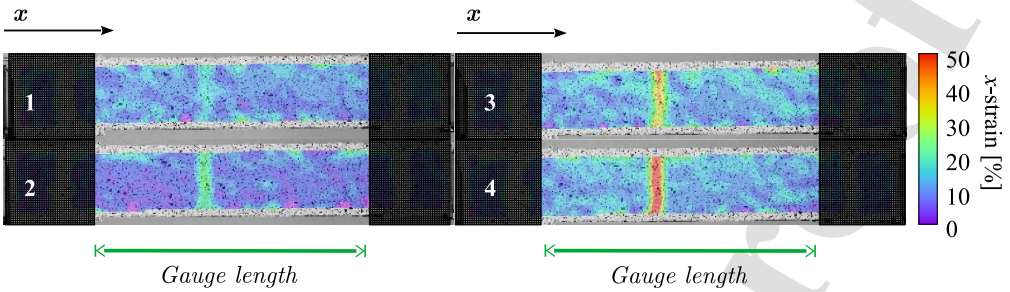

Figure 18: Cracking development for B-UC-1 specimen

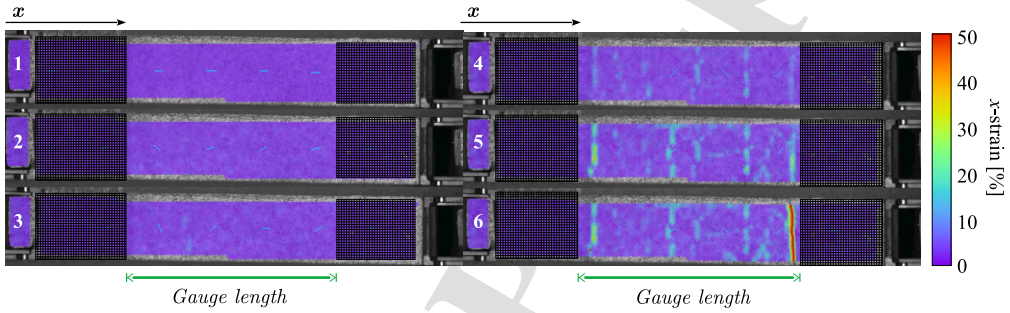

Figure 19: Cracking development for B-RHA-4 specimen

"B-RHA-4". This diffused crack pattern is also associated with the absence of telescopic failure, as already observed for epoxy-coated TRM [12, 54].

Figure 20 gives additional information by showing the post-failure appearance of the specimens. Indeed, it compares the typical behaviour of coated and uncoated specimens, specifically with regard to B-TRM, although similar considerations also apply to G-TRM. In general, uncoated specimens experience more and more damage in the vicinity of the first crack. The first crack is randomly located along the gauge length, as a consequence of the stochastic presence of microstructural defects. Conversely, multiple diffuse cracks can be clearly observed in the specimens reinforced with coated textiles. For the coated samples, failure is originated by moderate crack widening, often in proximity to the tabs, or in

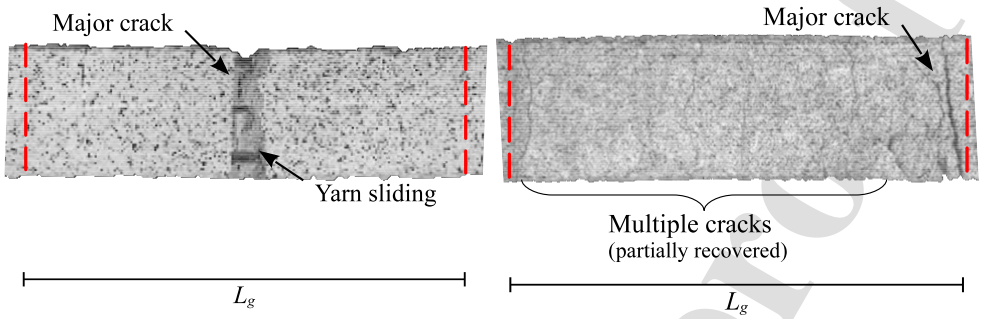

(a) B-NC (b) B-RHA

Figure 20: Typical failure modes showcased by uncoated and coated samples after testing

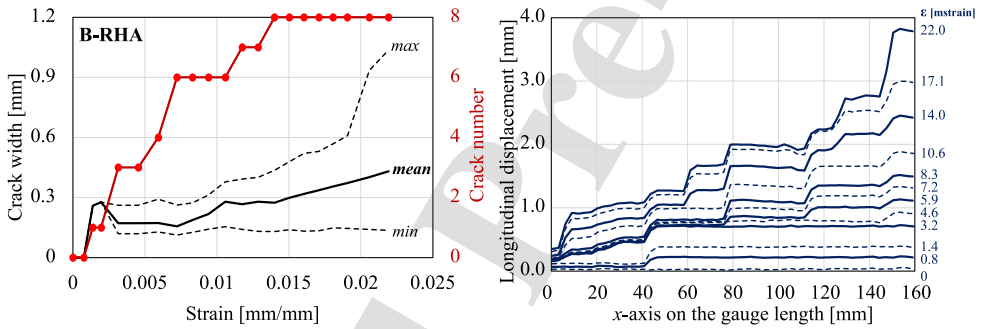

(a) Displacement along the mid-line (b) Crack width (left) and number (right scale)

Figure 21: Crack width and number development during testing for B-RHA-4 specimen

the middle of the gauge length. As the applied load increases, additional cracks open while pre-existing ones widen, until brittle failure of the textile occurs at the weakest crack [55, 32]. Upon failure of the textile, partial recovery in the diffuse crack pattern is experienced.

3.3.4. Crack analysis

Investigation of the crack pattern provides many indications of the bonding quality.

In particular, Figure 21 illustrates the crack analysis of a coated B-TRM spec-

imen and shows (a) the longitudinal displacement profile at different stages of the test, and (b) the resulting crack width and crack number. It can be noted that several micro-cracks develop during the test. In fact, the average crack width remains constant as new cracks are being generated, and this can only occur if the textile is able to transfer significant load along short (longitudinal) distance. This enables an enhanced bearing capacity that is reflected by the strain-hardening nature of the response. At the same time, as the strain increases, the crack number increases very rapidly at first, but then stabilises and remains almost constant. In fact, only a few cracks form outside the linear elastic stage. Then, pre-existing cracks widen until catastrophic failure is attained upon textile rupture [56].

4. CONCLUSIONS

In this paper, we discuss mechanical performance of textile reinforced mortar (TRM) composites reinforced by alkali resistant glass (G) or basalt (B) woven textiles. In particular, spotlight is set on the benefits associated with treating the textiles' surface with a special epoxy-based coating carrying rice husk ash (RHA) powder as filler. This approach aims specifically at modifying the interface zone between the hydraulic matrix and the textile, improving the bond quality. Three RHA powders are considered, which differ by the origin of the rice husks and by the temperature of the combustion process. Additionally, an extra RHA powder is studied which is obtained from the as-received RHA by milling and sieving below 100 μm. Results are discussed against undensified silica fume (SF), whose role as benchmark is justified by its popularity as pozzolanic additive. All powders are assessed in terms of specific surface area and amorphous silica content. Following the relevant guidelines [28, 33], mechanical performance is determined by uni-axial tensile testing of rectangular TRM coupons, with and without coating.

During testing, the cracking pattern evolution is monitored through digital image correlation (DIC). The following conclusions may be drawn:

- RHA powders obtained at low temperature exhibit higher contents of amorphous silica. Indeed, as already reported in the literature, high temperature incineration promotes crystallisation of silica polymorphs, especially tridymite and cristobalite.

- The RHA powder obtained by blending white and parboiled rice husk (powder “GA-RHA") exhibits the greatest application potential, in light of its wide specific surface area (SSA) and high amorphous silica content.

- Milling of this RHA is advisable, because the particle size of the as-received powder is relatively coarse (d_{50} around 212 μm) and unsuitable for coating deposition. After milling, the average particle size is about half of that of SF (d_{50} around 7 μm for milled GA-RHA, against 12 μm for SF), despite the particle size distribution of SF remaining slightly narrower. As a downside, milling damages the delicate comb-like microstructure of the original RHA powder, which is responsible for its exceptionally high SSA. Consequently, milling slightly reduces the SSA compared to the original powder. Still, the SSA remains three times as much as that of SF.

- Owing to weak bonding between at the matrix-textile interface, TRM specimens whose reinforcement has not received the RHA/epoxy coating display an inconsistent failure mode. Failure is initiated by brittle fracture of the mortar matrix, followed by friction-dominated delamination and/or telescopic failure. In this sense, uncoated specimens are unable to fully exploit the potential of the reinforcing textile and mechanical performance is almost

insensitive to the textile's nature, be it basalt or glass. The stress-strain behaviour is softening or, occasionally, perfect plastic and then softening.

- Application of the hybrid coating substantially improves adhesion between the textile and the hydraulic matrix, which fact results in a pronounced strain hardening regime. Failure occurs consistently through textile rupture, after diffuse cracking appears in the matrix. Inspection of failed specimens reveals diffused patches of mortar well attached to the textile yarns and no occurrence of telescopic failure.

- In terms of ultimate tensile strength and energy dissipation capability, this RHA/epoxy coating offers remarkable improvements. In particular, for the TRM composites with basalt textiles, the mean tensile strength is three times as much as the uncoated specimens, whereas the dissipated energy at failure is nearly four times as much. Interestingly, the adoption of the RHA/epoxy coating is especially effective for basalt textiles, given that their intrinsic tensile strength is far superior to that of glass textiles. Nonetheless, the effect of coating on glass textile-reinforced TRMs remains noticeable, with a 35% increase in tensile strength. Yet, the main advantage for glass textiles is expressed in terms of energy dissipated at failure, which exhibits a three-fold increase. This suggests that the coating is mainly beneficial in terms of ductility when relatively weak fibres are used. Also, its role in proctecting the textiles from the strongly alkaline environment should not be underestimated, especially for basalt fibres.

ACKNOWLEDGEMENTS

The Authors are grateful to Dr. Valentina Lugano (Curtiriso S.r.l.) and to Ing. Giorgia Martinelli (Kerakoll S.p.A.) for providing the rice husk ash powders and the lime mortar, respectively. The technical assistance by Dr. Miriam Hanusková (particle size analysis), Dr. Mauro Zapparoli (SEM and FEG-SEM imaging), and Dr. Massimo Tonelli (XRD analysis) is also gratefully acknowledged.

CRediT author statement

Cesare Signorini: Conceptualization, Methodology, Formal analysis, Investigation, Visualization, Data Curation, Writing - Original Draft, Writing - Review & Editing. **Antonella Sola**: Conceptualization, Methodology, Validation, Visualization, Writing - Original Draft, Writing - Review & Editing; **Andrea Nobili**: Writing - Review & Editing, Visualization, Funding Acquisition.

Funding

This research has been performed within the framework of the grant MIUR-PRIN 2020F3NCPX "Mathematics for industry 4.0 (Math4I4)". Also, support by "Progetto IMPReSA", within the framework POR-FESR 2014/2020 - asse 1.2.2, [CUP E81F18000310009], is gratefully acknowledged.

Ethics in publishing

The Authors adhere to the Ethics in publishing of this Journal.

REFERENCES

[1] F. J. De Caso y Basalo, F. Matta, A. Nanni, Fiber reinforced cement-based composite system for concrete confinement, Construction and Building Materials 32 (2012) 55–65.

[2] A. D'Ambrisi, L. Feo, F. Focacci, Experimental analysis on bond between PBO-FRCM strengthening materials and concrete, Composites Part B: Engineering 44 (2013) 524–532.

[3] R. Nadiv, A. Peled, V. Mechtcherine, S. Hempel, C. Schroefl, Micro-and nanoparticle mineral coating for enhanced properties of carbon multifilament yarn cement-based composites, Composites Part B: Engineering 111 (2017) 179–189.

[4] B. Banholzer, Bond of a strand in a cementitious matrix, Materials and structures 39 (2006) 1015–1028.

[5] A. Bentur, M. Y. Yardımcı, R. Tirosh, Preservation of telescopic bonding upon aging of bundled glass filaments by treatments with nano-particles, Cement and concrete research 47 (2013) 69–77.

[6] M. Butler, V. Mechtcherine, S. Hempel, Experimental investigations on the durability of fibre–matrix interfaces in textile-reinforced concrete, Cement and Concrete Composites 31 (2009) 221–231.

[7] M. Butler, V. Mechtcherine, S. Hempel, Durability of textile reinforced concrete made with AR glass fibre: effect of the matrix composition, Materials and structures 43 (2010) 1351–1368.

[8] C. Signorini, A. Nobili, Comparing durability of steel reinforced grout (SRG) and textile reinforced mortar (TRM) for structural retrofitting, Materials and Structures 54 (2021) 1–15.

[9] ACI PRC-549.6-20, Guide to Design and Construction of Externally Bonded Fabric-Reinforced Cementitious Matrix (FRCM) and Steel-Reinforced Grout (SRG) Systems for Repair and Strengthening Masonry Structures, American Concrete Institute, 2020.

[10] E. G. Daskiran, M. M. Daskiran, M. Gencoglu, Development of fine grained concretes for textile reinforced cementitious composites, Computers and Concrete 18 (2016) 279–295.

[11] J. Donnini, V. Corinaldesi, A. Nanni, Mechanical properties of FRCM using carbon fabrics with different coating treatments, Composites Part B: Engineering 88 (2016) 220–228.

[12] M. Messori, A. Nobili, C. Signorini, A. Sola, Mechanical performance of epoxy coated AR-Glass fabric Textile Reinforced Mortar: Influence of coating thickness and formulation, Composites Part B: Engineering 149 (2018) 135–143.

[13] D. Dvorkin, A. Poursaee, A. Peled, W. J. Weiss, Influence of bundle coating on the tensile behavior, bonding, cracking and fluid transport of fabric cement-based composites, Cement and Concrete Composites 42 (2013) 9–19.

[14] C. Scheffler, S. Gao, R. Plonka, E. Mäder, S. Hempel, M. Butler, V. Mechtcherine, Interphase modification of alkali-resistant glass fibres and carbon fibres for textile reinforced concrete I: Fibre properties and durability, Composites Science and Technology 69 (2009) 531–538.

[15] M. Messori, A. Nobili, C. Signorini, A. Sola, Effect of high temperature exposure on epoxy-coated Glass Textile Reinforced Mortar (GTRM) composites, Construction and Building Materials 212 (2019) 765–774.

[16] C. Signorini, A. Nobili, A. Sola, M. Messori, Designing epoxy viscosity for optimal mechanical performance of coated glass textile reinforced mortar (GTRM) composites, Construction and Building Materials 233 (2020) 117325.

[17] Z. Cohen, A. Peled, Effect of nanofillers and production methods to control the interfacial characteristics of glass bundles in textile fabric cement-based composites, Composites Part A: Applied Science and Manufacturing 43 (2012) 962–972.

[18] C. Signorini, A. Sola, A. Nobili, C. Siligardi, Lime-cement textile reinforced mortar (TRM) with modified interphase, The Journal of Applied Biomaterials and Functional Materials 17 (2019). doi:10.1177/2280800019827823.

[19] C. Signorini, A. Nobili, Targeting functionalised carbon nanotubes at the interphase of textile reinforced mortar (TRM) composites, Composites Part A: Applied Science and Manufacturing 144 (2021) 106330.

[20] P. Di Maida, C. Sciancalepore, E. Radi, F. Bondioli, Effects of nano-silica treatment on the flexural post cracking behaviour of polypropylene macro-synthetic fibre reinforced concrete, Mechanics Research Communications 88 (2018) 12–18.

[21] C. Signorini, A. Sola, B. Malchiodi, A. Nobili, Highly dissipative fiber-reinforced concrete for structural screeds, Journal of Materials in Civil Engineering 34 (2022) 04022022.

[22] N. Baccile, F. Babonneau, B. Thomas, T. Coradin, Introducing ecodesign in silica sol–gel materials, Journal of Materials Chemistry 19 (2009) 8537–8559.

[23] V. Sata, C. Jaturapitakkul, K. Kiattikomol, Influence of pozzolan from various by-product materials on mechanical properties of high-strength concrete, Construction and Building Materials 21 (2007) 1589–1598.

[24] K. Ganesan, K. Rajagopal, K. Thangavel, Rice husk ash blended cement:

Assessment of optimal level of replacement for strength and permeability properties of concrete, Construction and building materials 22 (2008) 1675–1683.

[25] S. Demis, J. Tapali, V. Papadakis, An investigation of the effectiveness of the utilization of biomass ashes as pozzolanic materials, Construction and Building Materials 68 (2014) 291–300.

[26] A. Sola, C. Signorini, M. Hanuskova, M. Zapparoli, Preliminary assessment of rice husk ash (RHA) as functional interphase agent in sustainable composite systems for structural strengthening, in: Key Engineering Materials, volume 919, Trans Tech Publ, 2022, pp. 98–107.

[27] GeoCalce® F Antisismico, Kerakoll Spa, 2020. https://products.kerakoll.com/yep-repository/kerakoll/media/GeoCalce_F_Antisismico_0418_chit.pdf.

[28] ICC AC434, Acceptance criteria for masonry and concrete strengthening using fiber-reinforced cementitious matrix (FRCM) composite systems, Technical Report, International Code Council, 2013.

[29] C. Signorini, A. Nobili, F. O. Falope, Mechanical performance and crack pattern analysis of aged Carbon Fabric Cementitious Matrix (CFRCM) composites, Composite Structures 202 (2018) 1114 – 1120. Special issue dedicated to Ian Marshall.

[30] Mastersizer 2000 User Manual + addendum, Malvern Panalytical, 2023. https://www.malvernpanalytical.com/en/assets/Mastersizer-2000-user-manual-English-MAN0384-1-0_tcm50-11674.pdf. Last accessed on February 9, 2023.

[31] J. Hartig, F. Jesse, K. Schicktanz, U. Häußler-Combe, Influence of experi-

mental setups on the apparent uniaxial tensile load-bearing capacity of textile reinforced concrete specimens, Materials and Structures 45 (2012) 433–446.

[32] F. Nerilli, B. Ferracuti, A tension stiffening model for FRCM reinforcements calibrated by means of an extended database, Composite Structures 284 (2022) 115100.

[33] RILEM 232-TDT, Test methods and design of textile reinforced concrete, Technical Report 12, International Union of Laboratories and Experts in Construction Materials, Systems and Structures, 2016. doi:10.1617/s11527-016-0839-z.

[34] F. Focacci, T. D'Antino, C. Carloni, The role of the fiber–matrix interfacial properties on the tensile behavior of FRCM coupons, Construction and Building Materials 265 (2020) 120263.

[35] L. Chauvaud, A. Lorrain, R. B. Dunbar, Y.-M. Paulet, G. Thouzeau, F. Jean, J.-M. Guarini, D. Mucciarone, Shell of the great scallop pecten maximus as a high-frequency archive of paleoenvironmental changes, Geochemistry, Geophysics, Geosystems 6 (2005).

[36] A. C. Kumpfer Nascimento, Study of rice husk ash by infrared spectroscopy, International Journal of Science and Engineering Investigations 9 (2020).

[37] A. Rivas, G. Vera, V. Palacios, A. Rigail, M. C. Martinez, Characterization of rice husk and the crystallization process of amorphous silica from rice husk ash, in: Conference on 14th LACCEI International Multi-Conference for Engineering, Education, and Technology, 2016. doi:10.18687/LACCEI2016.1.1.093.

[38] Y. Shinohara, N. Kohyama, Quantitative analysis of tridymite and cristobalite crystallized in rice husk ash by heating, Industrial health 42 (2004)

277–285.

[39] R. K. Biswas, P. Khan, S. Mukherjee, A. K. Mukhopadhyay, J. Ghosh, K. Muraleedharan, Study of short range structure of amorphous silica from pdf using ag radiation in laboratory XRD system, raman and nexafs, Journal of Non-Crystalline Solids 488 (2018) 1–9.

[40] K. Arroudj, A. Zenati, M. N. Oudjit, A. Bali, A. Tagnit-Hamou, Reactivity of fine quartz in presence of silica fume and slag, Engineering 3 (2011) 569.

[41] C. Cárdenas-Escudero, V. Morales-Flórez, R. Pérez-López, A. Santos, L. Esquivias, Procedure to use phosphogypsum industrial waste for mineral CO_2 sequestration, Journal of Hazardous Materials 196 (2011) 431–435.

[42] European Silica Fume Committee, Characterization of silica fume. composition, 2022. URL: `http://www.microsilicafume.eu/page/composition_silica_fume_amorphous_silicon_dioxide/f1.html`, last accessed August 22, 2022.

[43] P. Chindaprasirt, S. Rukzon, V. Sirivivatnanon, Resistance to chloride penetration of blended portland cement mortar containing palm oil fuel ash, rice husk ash and fly ash, Construction and Building Materials 22 (2008) 932–938.

[44] P. Mehta, The chemistry and technology of cements rice husk ash made from rice husk ash, in: Proc. UNIDO/Escap Workshop on Rice Husk Ash Cement, Peshawar, Pakistan, 1979, 1979.

[45] E. M. Hotze, T. Phenrat, G. V. Lowry, Nanoparticle aggregation: challenges to understanding transport and reactivity in the environment, Journal of environmental quality 39 (2010) 1909–1924.

[46] B. A. Tayeh, R. Alyousef, H. Alabduljabbar, A. Alaskar, Recycling of rice

husk waste for a sustainable concrete: a critical review, Journal of Cleaner Production 312 (2021) 127734.

[47] M. Jamil, M. Khan, M. Karim, A. Kaish, M. Zain, Physical and chemical contributions of rice husk ash on the properties of mortar, Construction and Building Materials 128 (2016) 185–198.

[48] D. A. S. Rambo, F. de Andrade Silva, R. D. Toledo Filho, O. d. F. M. Gomes, Effect of elevated temperatures on the mechanical behavior of basalt textile reinforced refractory concrete, Mater Design 65 (2015) 24–33.

[49] J. P. M. Arias, C. Bernal, A. Vázquez, M. M. Escobar, Aging in water and in an alkaline medium of unsaturated polyester and epoxy resins: experimental study and modeling, Advances in Polymer Technology 37 (2018) 450–460.

[50] Minimising Energy in Construction, Characteristic values, n.d. URL: https://www.meicon.net/95-values, last accessed August 24, 2022.

[51] V. C. Li, H. Stang, Interface property characterization and strengthening mechanisms in fiber reinforced cement based composites, Advanced Cement Based Materials 6 (1997) 1–20.

[52] J. Donnini, V. Corinaldesi, Mechanical characterization of different FRCM systems for structural reinforcement, Construction and Building Materials 145 (2017) 565–575.

[53] M. E. A. Fidelis, F. de Andrade Silva, R. D. Toledo Filho, The influence of fiber treatment on the mechanical behavior of jute textile reinforced concrete, in: Key Engineering Materials, volume 600, Trans Tech Publ, 2014, pp. 469–474.

[54] S. Guo, J. Ren, T. Yang, M. Z. Rahman, C. Shi, D. Zhu, Influences of sur-

face treatment on the mechanical performances of carbon and basalt textiles-reinforced concretes under harsh environments, Composites Part B: Engineering 246 (2022) 110195.

[55] S. De Santis, G. de Felice, Tensile behaviour of mortar-based composites for externally bonded reinforcement systems, Composites Part B: Engineering 68 (2015) 401–413.

[56] U. Häußler-Combe, J. Hartig, Bond and failure mechanisms of textile reinforced concrete (TRC) under uniaxial tensile loading, Cement and concrete composites 29 (2007) 279–289.

Manuscript ID CCC-D-22-02269

Hierarchical composite coating for enhancing the tensile behaviour of textile-reinforced mortar (TRM)

by C. Signorini, A. Sola, A. Nobili

Highlights

1. A novel surface coating for textile-reinforced mortar composite system is proposed
2. The coating is epoxy-based and uses rice husk ash (RHA) particles as active filler
3. Three RHA powders are considered differing by rice variety and combustion process
4. Uniaxial tensile tests on basalt- and glass-TRM prismatic coupons are conducted
5. The coating leads to enhanced strength, toughness and crack pattern in TRM samples

Declaration of interests

☒ The authors declare that they have no known competing financial interests or personal relationships that could have appeared to influence the work reported in this paper.

☐ The authors declare the following financial interests/personal relationships which may be considered as potential competing interests: